INSTITUTE OF PLASMA PHYSICS

NAGOYA UNIVERSITY

NUMERICAL SIMULATION ON THE SCREW PINCH BY 2-D MHD PINCH CODE "TOPICS" INCLUDING IMPURITIES AND NEUTRALS EFFECTS

A. Nagata, H. Ashida*, M. Okamoto and K. Hirano

(Rceieved - Mar. 7, 1981)

IPPJ-512 March 1981

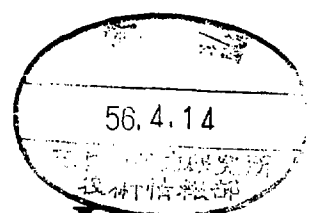

RESEARCH REPORT

NAGOYA, JAPAN

NUMERICAL SIMULATION ON THE SCREW PINCH BY 2-D MHD PINCH CODE "TOPICS" INCLUDING IMPURITIES AND NEUTRALS EFFECTS

A. Nagata, H. Ashida*, M. Okamoto and K. Hirano

(Rceieved - Mar. 7, 1981)

IPPJ-512 March 1981

Further information about this report is to be sent to the Research Information Center, Institute of Plasma Physics, Nagoya University, Nagoya 464, Japan.

* Electrotechnical Laboratory, Ibaraki 305, Japan.

ABSTRACT

Two dimensional fluid simulation code "TOPICS" is developed for the STP-2, the shock heated screw pinch at Nagoya. It involves the effects of impurity ions and neutral atoms. In order to estimate the radiation losses, the impurity continuity equations with ionizations and recombinations are solved simultaneously with the plasma fluid equations. The results are compared with the coronal equilibrium model. It is found that the coronal equilibrium model underestimates the radiation losses from shock heated pinch plasmas in its initial dynamic phase. The present calculations including impurities and neutrals show the importance of the radiation losses from the plasma of the STP-2. Introducing the anomalous resistivity caused by the ion acoustic instability, the observed magnetic field penetration is explained fairly well.

1. INTRODUCTION

Toroidal pinch apparatuses such as screw pinches, belt pinches and reversed field pinches have been expected to produce higher beta plasmas than that attained by usual ohmically heated tokamaks. However, temperatures achieved so far in those machines are low compared with the expected value. It is very important to understand what physical conditions are responsible for the unexpected low temperature. In the present paper this problem is investigated through 2-D MHD code "TOPICS" [1,2] using the experimental results of the STP-2 [3]. Two dimensional treatment is important for the screw pinch because high beta effects create complex two-dimensional motion such as plasma distortion from circular cross-section and large toroidal drift from the center of the discharge tube. Main efforts are paid to include impurity and neutral particles effects in "TOPICS" since they are thought to be critically important for drastic energy loss from shock heated pinch plasmas. In the past these problems are treated rather incompletely by several authors. Becker and Düches [4] treated them precisely in their 1-D MHD code but the application to the implosion phase is not possible. Byrne and Chu [5] wrote them up in their 1-D but one fluid MHD code, and moreover they assume the coronal equilibrium model which is not a very good approximation for the early phase of the fast toroidal pinch as is pointed out by Post [6]. Sgro and Nielson's work [7] is 1-D hybrid code so that it is not always convenient to study longer time events than 5 μsec. We believe that shortcomings of the former works can be improved in the present paper since we added rate equations of impurities and neutral particle effect of the working gas.

In section 2, we describe the basic MHD equations and the transport

coefficients used in the TOPICS. Computational models for impurity ions and neutral atoms are presented in sections 3 and 4, respectively. In section 5, we compare the simulated results with the experimental results of the STP-2, which clearly shows the importance of the energy loss due to impurity ions and neutral atoms and the anomalous resistivity.

2. BASIC EQUATIONS AND TRANSPORT COEFFICIENTS

The two-dimensional MHD toroidal pinch simulation code, TOPICS, is based on the MHD equations in addition to Ohm's law and Maxwell's equations. The MHD equations comprize the equations of continuity, momentum and the heat balance for electrons and ions. By using c.g.s. gauss units, all sets of equations are written as

$$\frac{\partial}{\partial t} n + \mathrm{div}\, n\vec{V} = 0 \ , \tag{2.1}$$

$$\frac{\partial}{\partial t} \rho\vec{V} + \mathrm{div}\, \rho\vec{V}\vec{V} = - \mathrm{grad}(P_i + P_e + nq_i) + \frac{1}{c} \vec{J} \times \vec{B} \ , \tag{2.2}$$

$$\frac{\partial}{\partial t} P_i + \mathrm{div}\, P_i\vec{V} = -(\gamma - 1)(P_i + nq_i)\, \mathrm{div}\, \vec{V}$$

$$+ (\gamma - 1)\mathrm{div}(\overleftrightarrow{\kappa}_i \ \mathrm{grad}\ T_i) + (P_e - ZP_i)/\tau_{eq} \ , \tag{2.3}$$

$$\frac{\partial}{\partial t} P_e + \mathrm{div}\, P_e\vec{V} = - (\gamma - 1)P_e \ \mathrm{div}\ \vec{V} + (\gamma - 1)\ \vec{J}\overleftrightarrow{\eta}\vec{J}$$

$$+ (\gamma - 1)\mathrm{div}(\overleftrightarrow{\kappa}_e \ \mathrm{grad}\ T_e) - (P_e - ZP_i)/\tau_{eq}$$

$$+ (\gamma - 1)P_{To} + n_e \cdot \Delta^* T_e \ , \tag{2.4}$$

$$\vec{E} = -\frac{1}{c}\left(\vec{V} - \frac{1}{en_e}\vec{J}\right) \times \vec{B} + \overleftrightarrow{\eta}\vec{J} - \frac{1}{en_e}\,\mathrm{grad}\,P_e\ , \qquad (2.5)$$

$$\frac{\partial}{\partial t}\vec{B} = -\,c\ \mathrm{rot}\ \vec{E}\ , \qquad (2.6)$$

$$\vec{J} = \frac{c}{4\pi}\,\mathrm{rot}\ \vec{B}\ , \qquad (2.7)$$

$$\mathrm{div}\ \vec{B} = 0\ . \qquad (2.8)$$

Here, Eq.(2.1) represents the particle conservation law for ions, where n and $\vec{V}$ are the ion density and the fluid velocity, respectively. The electron density is given by $n_e = Zn$ with Z the charge number.

Equation (2.2) is the momentum conservation law and ρ is the mass density given by $\rho = nm_i$, where m_i is the ion mass. Equations (2.3) and (2.4) represent the energy conservations for ions and electrons. In Eqs.(2.3) and (2.4), T_i and T_e are the ion and electron temperatures, respectively, $P_i = nT_i$ represents the ion pressure and $P_e = ZnT_e$ is the electron pressure. The terms of P_{To} and $n_e \cdot \Delta^* T_e$ in Eq.(2.4) respesent the electron energy losses due to impurity ions and neutral atoms, which are given by Eqs.(3.18) and (4.17), respectively. Equation (2.5) is Ohm's law, where the electron inertia and the thermal force are neglected. Equations (2.6)-(2.8) are Maxwell's equations, where $\vec{B}$ denotes the magnetic flux density, $\vec{E}$ is the electric field strength, and $\vec{J}$ represents the current density. In Eqs.(2.1)-(2.8), γ is the ratio of specific heat and c the speed of light. Transport coefficients $\overleftrightarrow{\kappa}_i$, $\overleftrightarrow{\kappa}_e$, τ_{eq} and $\overleftrightarrow{\eta}$ in Eqs.(2.3)-(2.5) represent ion and electron thermal conductivities, the energy equipartition time between electrons and ions, and the electric resistivity, respectively. It is

necessary to use the artificial viscosity q_i in Eqs.(2.2) and (2.3) so as to obtain a stable numerical solution through the shock front. Since neutral atoms and impurity ions give significant effects on the plasma behavior, it is important to take them into account in the transport coefficients $\overleftrightarrow{\kappa}_i$, $\overleftrightarrow{\kappa}_e$, and $\overleftrightarrow{\eta}$. We also consider the anomalies in the resistivity $\overleftrightarrow{\eta}$. We assume that they can be described by

$$\eta_{\alpha\beta} = \begin{cases} (\eta_{\parallel} - \eta_{\perp}) \dfrac{B_\alpha B_\beta}{B^2} + \eta_{\perp} + \eta^N , & (\alpha = \beta) , \\ (\eta_{\parallel} - \eta_{\perp}) \dfrac{B_\alpha B_\beta}{B^2} , & (\alpha \neq \beta) , \end{cases} \tag{2.9}$$

$$\eta_{\parallel,\perp} = \eta^C_{\parallel,\perp} + \eta^A_{\parallel,\perp} , \tag{2.10}$$

$$1/\kappa_{\alpha\beta} = \begin{cases} 1/\{(\kappa_{\parallel} - \kappa_{\perp}) \dfrac{B_\alpha B_\beta}{B^2} + \kappa_{\perp}\} + 1/\kappa^N , & (\alpha = \beta) , \\ 1/\{(\kappa_{\parallel} - \kappa_{\perp}) \dfrac{B_\alpha B_\beta}{B^2}\} , & (\alpha \neq \beta) , \end{cases} \tag{2.11}$$

$$\kappa_{\parallel,\perp} = \kappa^C_{\parallel,\perp} , \tag{2.12}$$

where the superscript C designates classical contribution, N neutral effect, and A anomalous one, and the symbols $\parallel$ and $\perp$ indicate parallel and perpendicular components to the magnetic field, respectively, and α and β are components of the coordinate system.

The classical transport coefficients in Eqs.(2.3)-(2.12) can be written as follows:

$$\ell n\Lambda = \begin{cases} \ell n \dfrac{3}{2e^3} \left(\dfrac{k_B^3 T_e^3}{\pi Z^3 n}\right)^{1/2} , & (T_e \leq 5 \times 10^5\ ^\circ K) , \\ \ell n \dfrac{e^2}{\hbar c} \dfrac{c k_B T_e}{e^3} \left(\dfrac{3m_e}{\pi Z^3 n}\right)^{1/2} , & (T_e > 5 \times 10^5\ ^\circ K) , \end{cases} \tag{2.13}$$

$$\kappa_{\perp,i}^{C} = \frac{nT_i\tau_i}{m_i}\,(2x_i^2 + 2.645)/\Delta_i \ , \tag{2.14}$$

$$\kappa_{\parallel,i}^{C} = 3.906\,\frac{nT_i\tau_i}{m_i} \ , \tag{2.15}$$

$$\Delta_i = x_i^4 + 2.70\,x_i^2 + 0.677, \quad x_i = \omega_i\tau_i \ , \quad \omega_i = \frac{ZeB}{cm_i} \ , \tag{2.16}$$

$$\tau_i = \frac{3\sqrt{m_i}(k_BT_i)^{3/2}}{4\sqrt{\pi}\ \ell n\Lambda e^4Z^4n} \ , \tag{2.17}$$

$$\kappa_{\perp,e}^{C} = \frac{Z_{eff}nT_e\tau_e}{m_e}\,(\gamma_1'x_e^2 + \gamma_0')/\Delta_e \ , \tag{2.18}$$

$$\kappa_{\parallel,e}^{C} = \frac{Z_{eff}nT_e\tau_e}{m_e}\,\gamma_0 \ , \tag{2.19}$$

$$\eta_{\perp}^{C} = \frac{m_e}{e^2Z_{eff}n\tau_e}\left(1 - \frac{\alpha_1'x_e^2 + \alpha_0'}{\Delta_e}\right) \ , \tag{2.20}$$

$$\eta_{\parallel}^{C} = \frac{m_e}{e^2Z_{eff}n\tau_e}\,\alpha_0 \ , \tag{2.21}$$

$$\Delta_e = x_e^4 + \delta_1x_e^2 + \delta_0 \ , \quad x_e = \omega_e\tau_e \ , \quad \omega_e = \frac{eB}{cm_e} \ , \tag{2.22}$$

$$\tau_e = \frac{3\sqrt{m_e}(k_BT_e)^{3/2}}{4\sqrt{2\pi}\ \ell n\Lambda e^4Z_{eff}^2n} \ , \tag{2.23}$$

$$\tau_{eq}^{-1} = \frac{8\sqrt{2\pi m_e}\ e^4Z_{eff}^2n\ell n\Lambda}{3m_i(k_BT_e)^{3/2}} \ , \quad \left(\frac{m_e}{m_i}T_i \ll T_e\right) \ , \tag{2.24}$$

where γ_0', γ_1', γ_0, α_1', α_0', α_0, δ_1 and δ_0 are functions of Z, which are given by Braginskii [8] and Z_{eff} is the effective ionic charge defined by Eq.(3.9). The other notations have usual meanings. For the anomalous

transport coefficeint, we adopt the following resistivity formula proposed by Chodura [9]:

$$\eta^{A}_{\perp,\parallel} = \frac{m_e}{e^2 n_e} \nu^{*}_{\perp,\parallel} \quad , \tag{2.25}$$

$$\nu^{*}_{\perp} = c_{\perp}\omega_{pi} \left[1 - \exp(-|V_{d\perp}|/f_{\perp}V_s)\right] , \tag{2.26a}$$

$$\nu^{*}_{\parallel} = c_{\parallel}\omega_{pi} \left[1 - \exp(-|V_{d\parallel}|/f_{\parallel}V_s)\right] , \tag{2.26b}$$

where ω_{pi} is the ion plasma frequency, $V_d = J/en$ is the drift velocity, $V_s = (\gamma k_B T_e/m_i)^{1/2}$ is the ion acoustic speed, and $c_{\perp,\parallel}$ and $f_{\perp,\parallel}$ are some numerical constants. The coefficients κ^{N}_{i}, κ^{N}_{e} and η^{N} due to collisions with neutrals will be described in section 4.

The basic equations including the transport coefficients mentioned above are solved numerically by the scheme of modified Lax-Wendroff method [1] in the pseudo-toroidal coordinate system shown in Fig.1.

3. NUMERICAL MODEL FOR IMPURITIES

In the present paper, only oxygen ions are taken into account and the velocity of impurity ions is assumed to be the same as that of the plasma. Impurity ions with various ionization stages are described by the rate equations,

$$\frac{\partial}{\partial t} n_k + \mathrm{div}\, n_k \vec{V} = n_e(\alpha_{k-1} n_{k-1} - \alpha_k n_k) - n_e(\beta_{k-1} n_k - \beta_k n_{k+1}) ,$$

$$(k = 1, 2, 3, \ldots, K) , \tag{3.1}$$

where n_k is the number density of impurity ions with (k-1) electric charge(s), and α_k is rate coefficients for ionization from the state k to (k+1) and β_k for recombination from (k+1) to k.

As for ionization rate coefficients α_k, we use the Lotz's formula [10] given by

$$\alpha_k = 6.7 \times 10^{-7} \sum_{j=1}^{N} \frac{a_{kj} q_{kj}}{T_e^{3/2}} \left\{ \frac{K_1(E_{kj}/T_e)}{E_{kj}/T_e} - \frac{b_{kj} \exp(c_{kj})}{E_{kj}/T_e + c_{kj}} K_1\left(\frac{E_{kj}}{T_e} + c_{kj}\right) \right\} ,$$

$$[\mathrm{cm}^3/\mathrm{sec}] , \qquad (3.2)$$

where T_e is in eV, E_{kj} is the ionization energy (in eV) of electrons in the j-th sub-shell of ion k, q_{kj} is the number of equivalent electrons in the j-th sub-shell and K_1 is the exponential integral given by $K_1(x) = \int_x^\infty \frac{e^{-t}}{t} dt$. The constants a_{kj}, b_{kj} and c_{kj} are proposed by Lotz, and N is the number of sub-shells contributing to ionization.

Total rate coefficients β_k for recombination from (k+1) to k are given by the sum of radiative recombination rate coefficients β_{rk} and di-electric recombination rate coefficients β_{dk};

$$\beta_k = \beta_{rk} + \beta_{dk} , \qquad [\mathrm{cm}^3/\mathrm{sec}] . \qquad (3.3)$$

For radiative recombination rate coefficients β_{rk} of impurity ions with k electric charge(s), we use the formula [10];

$$\beta_{rk} = 2.6 \times 10^{-14} (\beta_1 + \beta_2), \quad [\mathrm{cm}^3/\mathrm{sec}] , \qquad (3.4)$$

where

$$\beta_1 = k^2 \left(\frac{\chi_H}{T_e}\right)^{1/2} \frac{\mu_{k-1}}{n_{k-1}^3} \frac{E_{k-1}}{T_e} \exp(E_{k-1}/T_e) K_1(E_{k-1}/T_e) , \qquad (3.5a)$$

$$\beta_2 = 2k^2(\chi_H/T_e)^{1/2}\ \phi_{\ell+1}(k^2\chi_H/T_e)\ . \qquad (3.5b)$$

Here, χ_H = 13.6 eV is the ionization potential of hydrogen, E_{k-1} is the ionization potential of the ion after recombination and $\phi_{\ell+1}$ is the value tabled by Spitzer [11]. In Eq.(3.5), β_1 gives the contribution from the valence shell of the principal quantum number ℓ and β_2 represents recombination on the excited levels considered to be hydrogenic.

As for di-electric recombination rate coefficients β_{dk}, we also use the Vainshtein's formula [10];

$$\beta_{dk} = 1 \times 10^{-10} M(k)C(k)\left(\frac{E_T(k,1)}{T_e}\right)^{3/2} \exp(-E_T(k,1)/T_e)$$

$$[cm^3/sec]\ , \qquad (3.6)$$

where $E_T(k,1)$ is the energy (in eV) of the resonance transition 1 of ion k, and M(k) and C(k) represent coefficients depended on the type of the transition, which are given by the values in the Ref.[10].

Using rate coefficients α_k, β_k given by Eqs.(3.2) to (3.6), we can solve Eq.(3.1) by the splitting and fractional-step method [12]. The electron density n_e and the effective charge Z_{eff} are given by

$$n_e = Zn + \sum_k (k - 1)\ n_k\ . \qquad (3.7)$$

$$Z_{eff} = \{Z^2 n + \sum_k (k-1)^2 n_k\}/n_e \ . \qquad (3.8)$$

Radition losses due to impurities are Bremsstrahlung radiation loss P_{Br}, ionization loss P_{Io}, radiative recombination loss P_{Ra}, di-electronic recombination loss P_{Di} and line radiation loss P_{Li}, which are given by, respectively,

$$P_{Br} = 1.051 \times 10^{-13} Z_{eff}^2 n_e n_k T_e^{1/2} \ , \qquad [eV/cm^3 \cdot sec] \ , \quad (3.9)$$

$$P_{Io} = \sum_k n_e n_k \alpha_k (E_{kj} + \frac{3}{2} T_e) \ , \qquad [eV/cm^3 \cdot sec] \ , \quad (3.10)$$

$$P_{Ra} = \sum_k n_e n_k \beta_{rk} (E_{k-1} + \langle E_k \rangle) \ , \qquad [eV/cm^3 \cdot sec] \ , \quad (3.11)$$

$$P_{Di} = \sum_k n_e n_k \beta_{dk} (E_{k-1} + E_T) \ , \qquad [eV/cm^3 \cdot sec] \ , \quad (3.12)$$

$$P_{Li} = \sum_{k,j} n_e n_k \alpha_{kj}^{ex} \Delta E_{kj} \ , \qquad [eV/cm^3 \cdot sec] \ , \quad (3.13)$$

where $\langle E_k \rangle$ is the average energy of the captured electron given by the value in Ref.[13].

For excitation rate coefficients α_{kj}^{ex} in Eq.(3.13) we also use the Vainshtein's formula [10];

$$\alpha_{kj}^{ex} = 1 \times 10^{-8} \left(\frac{\chi_H E_{kj}}{\Delta E_{kj} E_{ko}}\right)^{3/2} \exp(-\beta) G_{kj}(\beta) \ , \quad [cm^3/sec] \ , \qquad (3.14)$$

where

$$\Delta E_{kj} = E_{ko} - E_{kj} \ , \qquad (3.15a)$$

$$\beta = \Delta E_{kj} / T_e \ , \qquad (3.15b)$$

$$G_{kj}(\beta) = \begin{cases} \dfrac{B_{kj}(\beta + 1)\beta^{1/2}}{\beta + \chi_{kj}} & \text{for} \quad \Delta S = 0 \text{ transitions,} \qquad (3.16a) \\ \dfrac{B_{kj}\,\beta^{3/2}}{\beta + \chi_{kj}} & \text{for} \quad \Delta S = 1 \text{ transitions.} \qquad (3.16b) \end{cases}$$

Here ΔE_{kj} is the excitation energy in eV, E_{ko} and E_{kj} give the ionization energies in eV of the lower and the upper levels, respectively, and ΔS represents the change of the spin and B_{kj} and χ_{kj} are given by the values in the Ref.[13]. Thus the total energy loss from the electrons are given by

$$P_{To} = -(P_{Br} + P_{Io} + P_{Ra} + P_{Di} + P_{Li}), \qquad [eV/cm^3 \cdot sec] \ . \qquad (3.17)$$

Here oxygen spectra of 33 lines [13] are taken into account to obtain line radiation losses. The calculated result of cooling rate for oxygen impurities is shown in Fig.2.

Radiation loss calculated by rate equations is compared with that by the coronal equilibrium model which is used in Byrne and Chu [5]. The difference in the calculated results is shown in section 5. In the coronal equilibrium model, i.e., steady state $\frac{d}{dt} n_k = 0$, Eq.(3.1) can be reduced to

$$n_k = \frac{\alpha_{k-1}}{\beta_{k-1}} n_{k-1} \ . \qquad (3.18)$$

We assume that initial and boundary conditions for impurity ions and neutral atoms are given by initial radial distributions,

$$n_{k,n}(r) = n_c \ , \qquad (3.19)$$

or

$$n_{k,n}(r) = n_1(e^{k_1 \frac{k}{a}} - 1) + n_c \ , \qquad (3.20a)$$

where

$$
\left.
\begin{aligned}
& n_1 = (n_w - n_c)/(e^{k_1} - 1) \ , \quad (k \neq 0) \ , \\
& n_{k,n}(0) = n_c \ , \\
& n_{k,n}(a) = \frac{n_w - n_c}{e^{k_1} - 1} (e^{k_1} - 1) + n_c = n_w \ , \\
& \langle n_{k,n} \rangle_{t=0} = \frac{n_w - n_c}{e^{k_1} - 1} \{ \frac{2}{k_1} (e^{k_1} - \frac{e^{k_1} - 1}{k_1}) - 1 \} + n_c \ ,
\end{aligned}
\right\} \quad (3.20b)
$$

Here, the suffix k and n represent impurity atoms and nuetrals, respectively, and n_c and n_w the impurity or neutral density at r = 0 and r = a, respectively, $\langle n_{k,n} \rangle_{t=0}$ is the initial averaged content of impurity ions or neutral atoms at time t = 0 and k_1 is a constant.

4. NUMERICAL MODEL FOR NEUTRAL ATOMS

In order to estimate the changes in the plasma density $\Delta^* n$ and the electron temperature $\Delta^* T_e$ caused by ionizations of neutral atoms, only rate equations are solved for neutral atoms, neglecting the motion of neutral atoms. It is assumed for simplicity that the temperature of neutral atoms is the same as that of plasma ions. Under the above conditions, continuity equations for ions and the rate equations for neutral atoms are expressed as

$$
\frac{\partial}{\partial t} n + \operatorname{div} n\vec{V} = \Delta^* n \ , \tag{4.1}
$$

$$
\begin{aligned}
\frac{\partial}{\partial t} n_n &= - \alpha_n n_e n_n + \beta_n n_e n \\
&= \Delta^* n_n = - \Delta^* n \ ,
\end{aligned} \tag{4.2}
$$

where n_n is the neutral density and α_n and β_n represent ionization and recombination rate coefficients for neutral atoms. Taking into account neutral atoms effects, Eq.(2.1) must be replaced by Eq.(4.1) as continuity equations for ions. The change in the electron temperature $\Delta^* T_e$ caused by electron-neutral collisions becomes

$$\Delta^* T_e = - \alpha_n n_n \{T_e + (\gamma - 1)\chi_H\} + (\gamma - 1)\beta_{cn}\chi_H n_e n$$

$$- (\gamma - 1)(\frac{4m_e}{m_i})\gamma_{en} n_n (T_e - T_n) , \qquad [eV/sec] \qquad (4.3)$$

where the first term on the right-hand side represents the ionization loss due to neutral atoms, the second term the collisional recombination loss, and the last one is the relaxation between electrons and neutral atoms. The coefficient γ_{en} in Eq.(4.3) is given by Düchs and Griem [14]:

$$\gamma_{en} = \sigma_o v_{rel}^{en} , \qquad [cm^3/sec] , \qquad (4.4)$$

where

$$\sigma_o = (\frac{47.4}{T_e(eV) + 1.3} + 2.14) \times 10^{-16} , \qquad [cm^2] , \qquad (4.5a)$$

$$v_{rel}^{en} = (\frac{8T_e(eV)}{\pi m_e})^{1/2} = 6.69 \times 10^7 T_e^{1/2}(eV) , \qquad [cm/sec] . \qquad (4.5b)$$

Here we employ formulae of ionization rate coefficients α_n in cm^3/sec given by Düchs, Post and Rutherford [15]. They are written by

$$\log_{10}\alpha_n = \begin{cases} -3.054x - 15.72\exp(-x) + 1.603\exp(-x^2) , \\ \qquad\qquad \text{for } T_e \leq 20 \text{ eV} , \qquad (4.6a) \\ -0.5151x - 2.563/x - 5.231 , \\ \qquad\qquad \text{for } T_e > 20 \text{ eV} , \qquad (4.6b) \end{cases}$$

where

$$x = \log_{10} T_e(\mathrm{eV}) \ . \tag{4.7}$$

As for recombination rate coefficients β_n, we use the ones by Düchs and Griem [14] which is expressed by the sum of radiative recombination rate coefficients β_{rn} and collisional ones β_{cn}, that is, we have

$$\beta_n = \beta_{rn} + n_e \beta_{cn} \ , \qquad [\mathrm{cm}^3/\mathrm{sec}] \ , \tag{4.8}$$

where

$$\beta_{rn} = 1.903 \times 10^{-14} \chi_H / \sqrt{T_e} \ , \tag{4.9a}$$

$$\beta_{cn} = 1.827 \times 10^{-27} / \chi_H^2 T_e (6.0 + T_e/\chi_H) \ . \tag{4.9b}$$

We also consider the electric resistivity η^N and thermal conductivities κ_i^N and κ_e^N which arise from the ion and electron collisions with neutral atoms. We employ the electric resistivity η^N, after Düchs and Griem [14]:

$$\eta^N = \frac{m_e}{e^2} \frac{n_n}{n_e} (\alpha_n + \sigma_o v_{rel}^{en}) \ . \tag{4.10}$$

Düchs and Griem [14] also give thermal conductivities κ_i^N and κ_e^N for ions and electrons of the form,

$$1/\kappa_i^N = \frac{n_n}{n_e} 0.8\sqrt{2} (\sigma_E + \sigma_u) \frac{4}{5} \frac{1}{k_B} \left(\frac{8}{\pi} \frac{T_i}{m_i}\right)^{-1/2} \ , \tag{4.11}$$

$$1/\kappa_e^N = \frac{1}{k_B} \frac{n_n}{n_e} \sigma_o \ 0.501 \left(\frac{T_e}{m_e}\right)^{-1/2} \ , \tag{4.12}$$

where

$$\sigma_E = \frac{2}{3} \pi d^2 + (2\pi\alpha e^2 \times 0.196/d^2)(2/\mu v_{rel}^2) \ , \qquad [\mathrm{cm}^2] \ , \tag{4.13a}$$

$$\sigma_u^{1/2} = 7.6 \times 10^{-8} - 1.06 \times 10^{-8} \log_{10}(T_i(eV)) \ , \quad [cm^2] \ , \quad (4.13b)$$

$$v_{rel} = \left(\frac{8}{\pi} \frac{T_i(eV)}{m_i}\right)^{1/2} = 1.562 \times 10^6 \ T_i^{1/2}(eV) \ , \quad [cm/sec] \ . \quad (4.13c)$$

Here α is the polarizability ($\alpha = 6.46 \times 10^{-25}$ cm^3), d is the gas-kinetic radius of neutral atoms ($d = 1.19 \times 10^{-8}$ cm) and μ represents the reduced mass.

Assuming that rate coefficients and the plasma parameters are constant during the time interval Δt, we obtain simple numerical schemes:

$$n_n(t + \Delta t) = \frac{\beta_n}{\alpha_n} n + \{n_n(0) - \frac{\beta_n}{\alpha_n} n\} \ e^{-\alpha_n n_e \Delta t} \ , \quad (4.14)$$

$$n_n(t) = n_n(0) \ , \quad (4.15)$$

$$\Delta^* n_n = - \Delta^* n = \frac{1}{\Delta t} \left[\frac{\beta_n}{\alpha_n} n + \{n_n(0) - \frac{\beta_n}{\alpha_n} n\} \ e^{-\alpha_n n_e \Delta t} - n_n(0)\right] \ , \quad (4.16)$$

$$\Delta^* T_e = - \alpha_n n\{T_e + (\gamma - 1)\chi_H\} + (\gamma - 1)\beta_{cn} \chi_H n_e n$$

$$- (\gamma - 1)\left(\frac{4m_e}{m_i}\right) \gamma_{en} n_n (T_e - T_n) \ , \quad (4.17)$$

$$n_n = n_n(t + \Delta t) \ . \quad (4.18)$$

The characteristic plasma parameters used in the present code are the averaged temperature $\langle T_{i,e} \rangle$, the averaged density $\langle n_{i,e} \rangle$, the poloidal beta β_p and the averaged toroidal beta $\langle \beta \rangle$, which are defined by, respectively,

$$\langle n_{i,e} \rangle = \frac{2}{\pi a^2} \int_0^{\pi} \int_0^{a} n_{i,e} r dr d\theta \ , \quad (4.19)$$

$$\langle T_{i,e} \rangle = \frac{2}{\langle n_{i,e} \rangle} \int_0^{\pi} \int_0^{a} n_{i,e} \cdot T_{i,e} r dr d\theta \ , \tag{4.20}$$

$$\beta_p = \frac{2}{\frac{B_p^2}{(2\mu_0)}} \int_0^{\pi} \int_0^{a} (n_e T_e + n_i T_i) r dr d\theta \ , \tag{4.21}$$

$$\langle \beta \rangle = 2\mu_0 \langle p \rangle / \langle B^2 \rangle \ , \tag{4.22}$$

where

$$\langle p \rangle = \frac{2}{\pi a^2} \int_0^{\pi} \int_0^{a} (n_e T_e + n_i T_i) r dr d\theta \ , \tag{4.23a}$$

$$\langle B^2 \rangle = \frac{2}{\pi a^2} \int_0^{\pi} \int_0^{a} (B_t^2 + B_p^2) r dr d\theta \ . \tag{4.23b}$$

Here B_t and B_p represent toroidal and poloidal components of the magnetic field, respectively.

5. SIMULATED RESULTS

First, numerical results obtained by solving rate equations given by Eq.(3.1) together with the equations given in section 2 are compared with those obtained by the coronal equilibrium calculation. As a typical example, we consider the Columbia Torus [5] with the initial bias field B_{to} = 1.0 kG, the maximum value of the toroidal magnetic field $B_{t\ max}$ = 1.2 T, the maximum value of the toroidal plasma current $I_{p\ max}$ = 120 kA, the initial uniform electron and ion temperatures $T_{io,eo}$ = 10 eV, the initial uniform electron density n_{eo} = 1 x 10^{15} cm^{-3}

and the oxygen impurity density of 1 x 10^{13} cm^{-3} which is initially distributed uniformly as neutrals. Time variations of the averaged electron temperature $<T_e>$ and the total radiation loss P_{total} is shown in Figs.3 and 4, respectively. The result without impurities is also shown in Fig.3. Total radiation loss calculated by the coronal equilibrium model is about three times less than that calculated by time dependent rate equations. The averaged electron temperature $<T_e>$ calculated by rate equations is 50 % smaller than that without impurities and decreases with time after the dynamic phase. On the other hand, the value of $<T_e>$ calculated by the coronal equilibrium model increases with time. It is clear that the corona equilibrium calculation underestimates the radiation loss. Accordingly, in the following calculations, the radiation loss due to impurity ions is calculated by continuity equations with rate equations (3.1).

Next, we use the TOPICS code for the analysis of experiments of the STP-2 apparatus [3]. The STP-2 has the ceramic or quartz discharge tube with the major radius of 25 cm and the minor radius of 9 cm. The shock heated high-beta plasma is produced by the fast rising toroidal magnetic field and the plasma current. Experiments were mainly done under the conditions of the toroidal magnetic field of 1.2 T with 6.0 micro-seconds rise, the initial toroidal bias field 100 G to 2.0 kG and the toroidal plasma current of 25 to 35 kA with 7.5 micro-seconds rise. Radial distributions of the electron temperature $T_e(r)$ are shown in Fig.5 under the following experimental parameters of the STP-2; the maximum value of the toroidal plasma current $I_{p\ max}$ = 26 kA, the initial uniform electron and ion temperatures $T_{io,eo}$ = 2.0 eV, and (a) the low initial bias field B_{to} = 270 G case and (b) the high initial bias field B_{to} = 2.0 kG case. In Fig.5, Cal.1 shows the result of the

calculation under the conditions that the initial plasma is fully ionized $n_{eo} = 2 \times 10^{14}$ cm^{-3}, and there is no impurity. Cal.2 is the case for the initial conditions of 5 % oxygen impurity and 25 % ionization degree of the initial plasma. The experimental data measured by ruby laser scattering are also shown. Four cases of calculated time evolution of $\langle T_e \rangle$ are shown in Fig.6, where Cal.3 is the case for the initial conditions of 1 % oxygen impurity and 25 % ionization degree of the initial plasma and Cal.4 indicates the results of the fully ionized initial plasma and 5 % oxygen impurity. The ionization degree of the initial plasma is measured to be 25 % by CO_2 laser interferometer. We also found that the contents of the oxygen impurity are fallen into the range of 1-5 % by the absolute spectroscopic intensity measurements of the oxygen impurity lines [16]. As is seen in Fig.5(a), temperature profiles in the case of the lower initial bias field B_{to} = 270 G drift toward the outer side of the discharge tube. However, in the case of the higher initial bias field B_{to} = 2.0 kG shown in Fig.5(b), the simulation shows the skin-like toroidal plasma current density distribution which agrees with the experimental profile of the hollow type. The averaged electron temperature $\langle T_e \rangle$ at t = 6 μs in the case of Cal.2 is about 50 % smaller that that of Cal.1, and is about 30 % smaller than that of Cal.4. It is seen in the simulation that the neutral atoms are fully ionized during 8 μs and the OIII line is dominant at t = 6 μs. The simulated results indicate that the ionization and radiation losses due to neutral atoms and impurity ions are the most important electron energy loss mechanism. The calculated results of Cal.2 agree well with the experimental results. Figure 7 shows time variation of the averaged toroidal beta value $\langle \beta \rangle$ for these parameters. The values of $\langle \beta \rangle$ in the case of Cals.1 and 4 decrease linearly during

the dynamic phase, and slow increase in $<\beta>$ of Cal.1 after the dynamic phase arises from the toroidal field decay after t = 6 μs and the increase in the electron temperature with time by Joule heating. The increase of other $<\beta>$ curves is reduced by the effects due to impurity ions and neutral atoms. The values of $<\beta>$ for Cals.2 and 3 at t = 6 μs are the half of that for the case of Cal.1. It is also found from Figs.(6) and (7) that the effect of the neutral atoms plays an important role in the electron energy loss during the initial dynamic phase and the radiation loss due to impurity ions is significant after the maximum compression.

For physical model of the magnetic field penetration, we employ resistivity algorithm described by Eqs.(2.25) and (2.26) in section 2. In Figs.8(a) and (b), radial distributions of the poloidal magnetic field $B_p(r)$ calculated by the classical and anomalous resistivities are compared with results measured by the magnetic probes at t = 4 and 6 μs. Constants of $C_{\perp,\parallel} = 0.125$ and $f_{\perp,\parallel} = 0.1$ are assumed in Eqs. (2.26a) and (2.26b) in the calculation. The position of the magnetic axis in 6 μs is about 2 cm outside the center of the tube, which agrees satisfactorily with the experimental value and the one calculated from Shafranov's formula. The poloidal magnetic field profiles in the region r = - 4 cm to 4 cm may be originated from the ambient current in the pre-ionization stage. The poloidal magnetic field calculated by the classical Spitzer resistivity shows a skin-like profile and the poloidal magnetic field does not penetrate into the plasma interior even at t = 6 μs. On the other hand, the poloidal magnetic fields penetrate if the anomalous resistivity is employed, and field profiles agree well with the experimental data obtained from the probe measurements as seen from Figs.8(a) and (b). Two fluid flow patterns at t = 4 μs projected

on the poloidal plane are shown in Figs.9(a) and (b). In the case of the classical transports, the fluid velocity pattern shows a strong outward movement, since the plasma is expanding at t = 4 μs. The fluid velocity calculated by using the anomalous resistivity is smaller than that by the classical resistivity, since the poloidal magnetic field has already penetrated at t = 4 μs.

6. CONCLUSIONS AND DISCUSSION

Two-dimensional pinch simulation code "TOPICS", which includes the effects of oxygen impurity and neutral atoms, is developed for the axisymmetric toroidal pinch plasmas with a circular cross-section. It is found that the coronal equilibrium model underestimates the radiation loss and continuity equations for impurity ions should be solved including time dependent rate equations. It is also found that the effect of neutral atoms plays an important role in the electron energy loss during the initial pinch phase and the radiation loss due to impurity ions becomes significant after the maximum compression. Simulated results with impurity ions of 5 % in deuterium filling gas with the 25 % ionization degree of the initial plasma agree well with the experimental measurements of the STP-2 high-beta pinch tokamak. For the interpretation of the field penetration, here the anomalous resistivity due to ion acoustic instability is introduced. As a result, the magnetic field penetration is well explained and a good agreement is obtained between the simulation and the experiment. We also consider the anomalous transports due to the lower hybrid drift instability. By using the simulation code with these effects, the plasma parameters of the shock heated pinch tokamak of STP-2 with the high plasma current

density ($I_{p\ max}$ = 140 kA) are investigated and are shown in Figs.10 and 11. Here, the plasma parameters of the initial electron density n_{eo} = (4-8) x 10^{14} cm^{-3} and the initial bias field B_{to} = (0-2) kG are assumed for the calculation. Dependence of the averaged temperature on the initial bias field is shown in Fig.10. Figure 11 shows effects of impurity ions and neutral atoms on the shock heated pinch plasma. A higher temperature plasma can be easily obtained by the control of the initial bias field at the initial phase. However, the electron temperature T_e in the case of 10 % initial ionization is 50 % smaller than that of the fully ionized case and in the case of 1 % oxygen impurity T_e is about 20 % smaller than that of the fully ionized case. The energy loss due to 1 % oxygen impurity or lower ionization degree of the initial plasma may be a serious problem in future experiments of a screw pinch and a shock heated pinch tokamak.

As the final remark, we notice that Hall terms appearing in the generalized Ohm's law Eqs.(2.5) may have significant effects in the dynamic phase of shock heated pinch plasmas, since the ratio of $\left|\frac{1}{en_e}\vec{J} \times \vec{B}\right|$ to $|\overleftrightarrow{\eta}\vec{J}|$ is $\sim \omega_e\tau_e$, and its order of magnitude amounts to about 2 x 10^3 in our experimental parameters. Further, asymmetry of the magnetic field on the equatorial plane may be caused by Hall effects and very complicated vortex may be formed in the plasma. However, in the present code, Hall effects cannot be taken into account because the symmetry of the upper and lower half planes are assumed. In order to investigate the Hall effects, the modified 2-D pinch simulation code is under development.

The authors would like to thank Professor T. Amano for useful comments on impurity study and Professor M. Wakatani for helpful discussions.

REFERENCES

[1] ASHIDA, H., in *Plasma Physics and Controlled Nuclear Fusion Research* (Proc. 5th Int. Conf. Tokyo, 1974) 3, IAEA, Vienna (1975) 481; and Bul. Electrotech. Lab. 41 (1977) 441.

[2] NAGATA, A., OKAMOTO, M., YAMAGUCHI, S., HIRANO, K., ASHIDA, H., *International Conference on Plasma Physics* (Proc. ICPP, Nagoya, 1980) 1 (1980) 148.

[3] HIRANO, K., KITAGAWA, S., SATO, K., WAKATANI, M., YAMADA, S., ARIMOTO, H., KITA, Y., YAMAGUCHI, S., NAGATA, A., in *Plasma Physics and Controlled Nuclear Fusion Research* (Proc. 7th Int. Conf. Innsbruck, 1978) 2, IAEA, Vienna (1979) 55.

[4] BECKER, G., DÜCHS, D.F., Nucl. Fusion 16 (1976) 763.

[5] BYRNE, R.N., CHU, C.K., Phys. Fluids 22 (1979) 2418.

[6] POST, D.E., *Symposium of Plasma Dynamics* (ed. F. H. Clauser, 1959) 30.

[7] SGRO, A.G., NIELSON, C.W., Phys. Fluids 19 (1976) 126.

[8] BRAGINSKII, S.J., "Transport Processes in a Plasma " in *Review of Plasma Physics* 1 (Consultants Bureau, 1965) 205.

[9] CHODURA, R., Nucl. Fusion 15 (1975) 55.

[10] BRETON, C., DE MICHELIS, C., MATTIOLI, M., Nucl. Fusion 16 (1976) 891.

[11] SPITZER, L., Jr., Astrophys. J. 107 (1948) 6.

[12] OKAMOTO, M., AMONO, T., J. Compt. Phys. 26 (1978) 80.

[13] MERCIER, C., code "MAKOKOT", TFR, 1977.

[14] DÜCHS, D.F., GRIEM, H.R., Phys. Fluids 9 (1966) 1099.

[15] DÜCHS, D.F., POST, D.E., RUTHERFORD, P.H., Nucl. Fusion 17 (1977) 565.

[16] YAMAGUCHI, S., private communication.

FIGURE CAPTIONS

Fig.1 Coordinate system.

Fig.2 Cooling rates for oxygen impurity.

Fig.3 Time variations of the averaged electron temperature calculated by using 100 % ionization degree of the initial plasma, the rate equations and the corona equilibrium model.

Fig.4 Time variations of the total radiation loss in the cases of the rate equations and the coronal equilibrium model.

Fig.5 Radial distributions of the electron temperature for the effects of impurity ions and neutral atoms in the cases of (a) the initial bias field B_{to} = 270 G and (b) B_{to} = 2 kG.

Fig.6 Time evolutions of the averaged electron temperature in the cases of Cal.1: 100 % ionization degree and without impurity, Cal.2: 5 % oxygen impurity and 25 % ionization degree, Cal.3: 1 % oxygen impurity and 25 % ionization degree, Cal.4: 100 % ionization degree and 5 % oxygen impurity.

Fig.7 Time variation of the averaged toroidal beta values under various conditions.

Fig.8 Radial distributions of the poloidal magnetic field calculated by the classical (— · —), anomalous (——) resistivities and the experiments (·) at (a) t = 4 μs and (b) t = 6 μs.

Fig.9 Velocity flow patterns on the poloidal plane at t = 4 μs in the cases of (a) the classical resistivity and (b) the anomalous resistivity.

Fig.10 Dependency of the averaged electron temperature on the initial bias field.

Fig.11 Effects of the impurity ions and neutral atoms in the shock heated pinch plasmas.

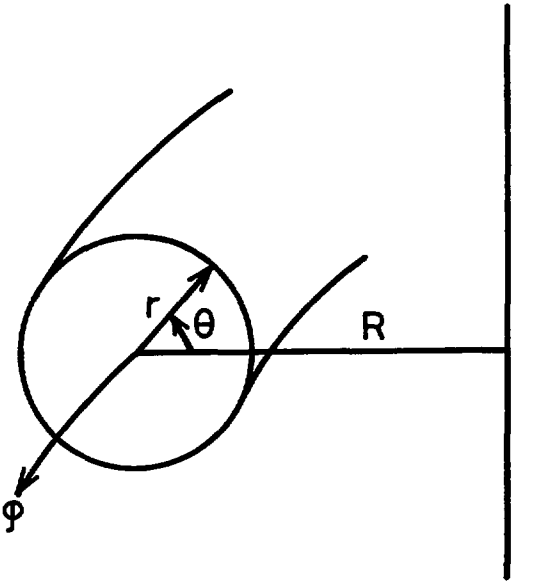

Fig. 1

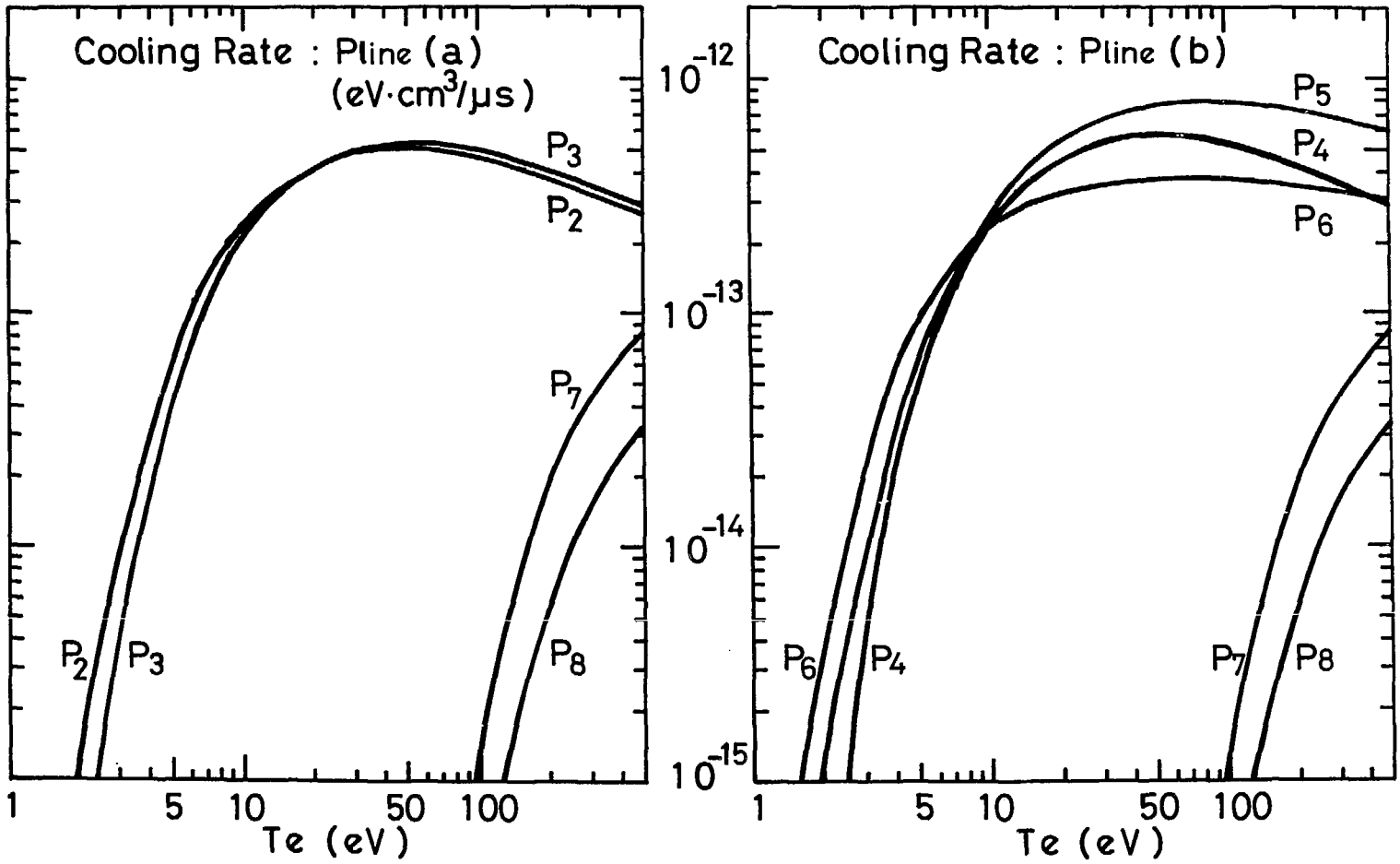
Cooling Rate : Pline (a)
(eV·cm³/μs)
P3
P2
P7
P8
P2
P3
1
5
10
50
100
Te (eV)
10⁻¹²
10⁻¹³
10⁻¹⁴
10⁻¹⁵
Cooling Rate : Pline (b)
P5
P4
P6
P6
P4
P7
P8
1
5
10
50
100
Te (eV)

Fig. 2

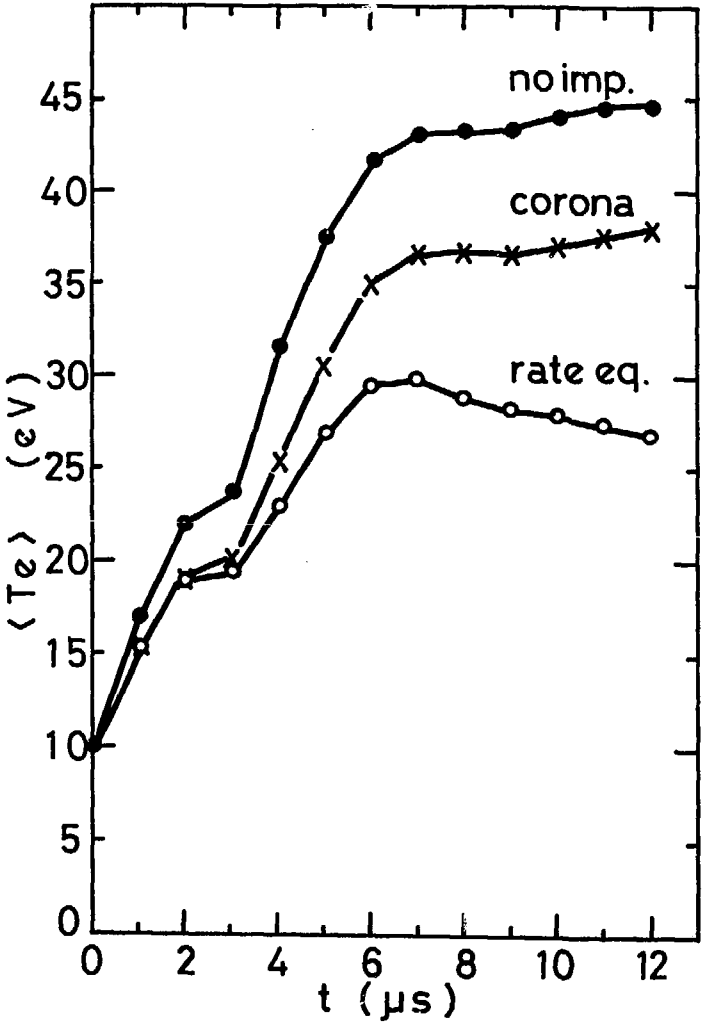
no imp.
corona
rate eq.
⟨Te⟩ (eV)
t (μs)
0
2
4
6
8
10
12
0
5
10
15
20
25
30
35
40
45

Fig. 3

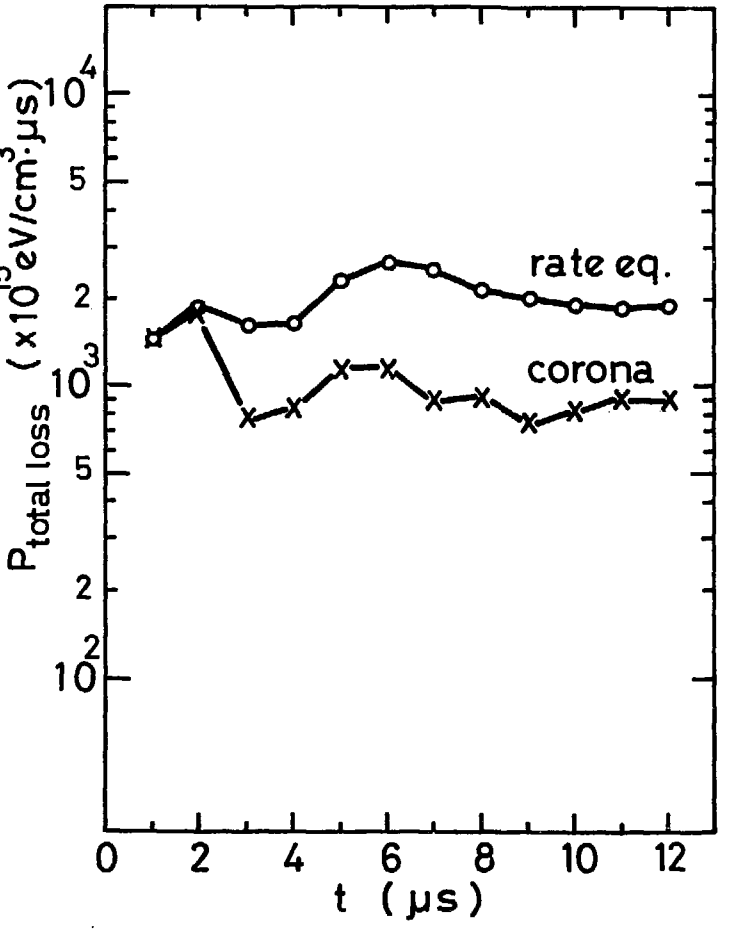
rate eq.
corona
$P_{total\ loss}$ ($\times 10^{15}$ eV/cm^3·μs)
t (μs)
0
2
4
6
8
10
12
10^2
2
5
10^3
2
5
10^4

Fig. 4

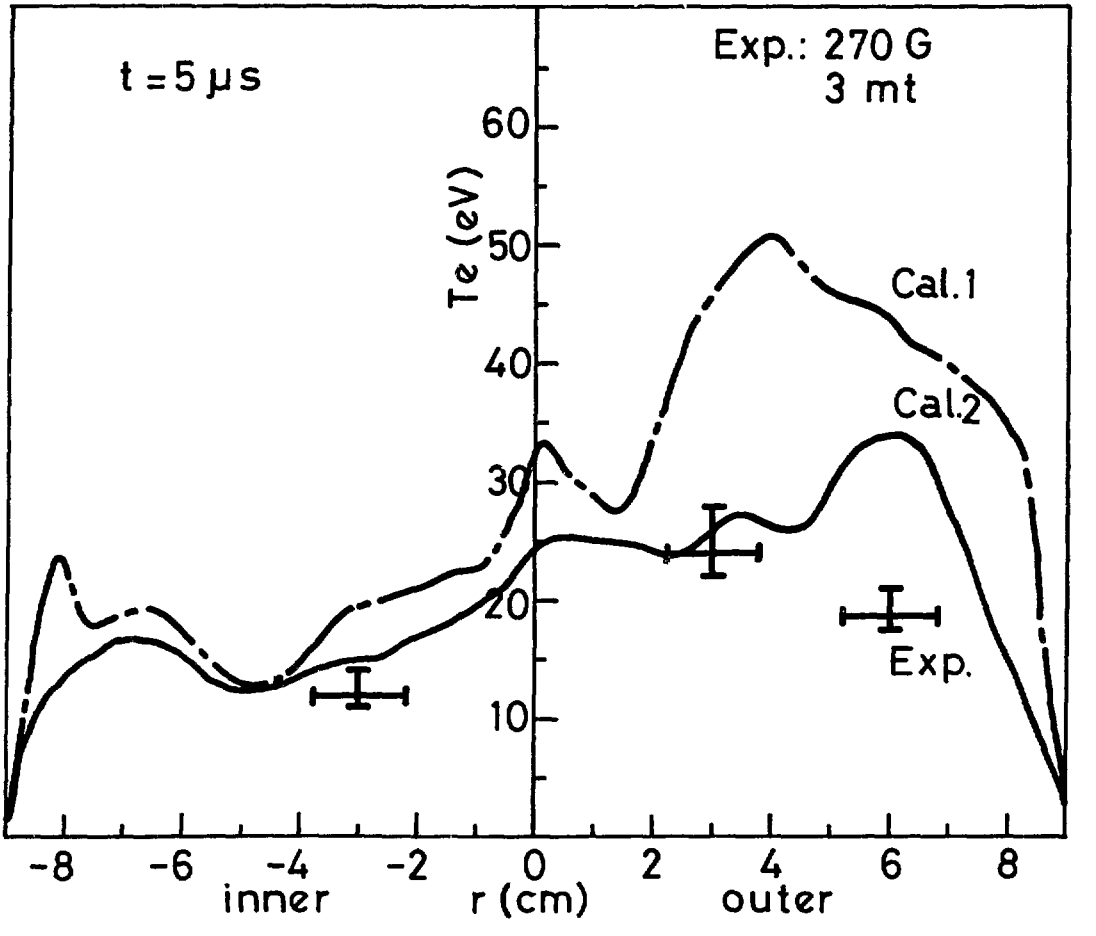
t = 5 μs
Exp.: 270 G
3 mt
Te (eV)
60
50
40
30
20
10
Cal.1
Cal.2
Exp.
-8
-6
-4
-2
0
2
4
6
8
inner
r (cm)
outer

Fig. 5 (a)

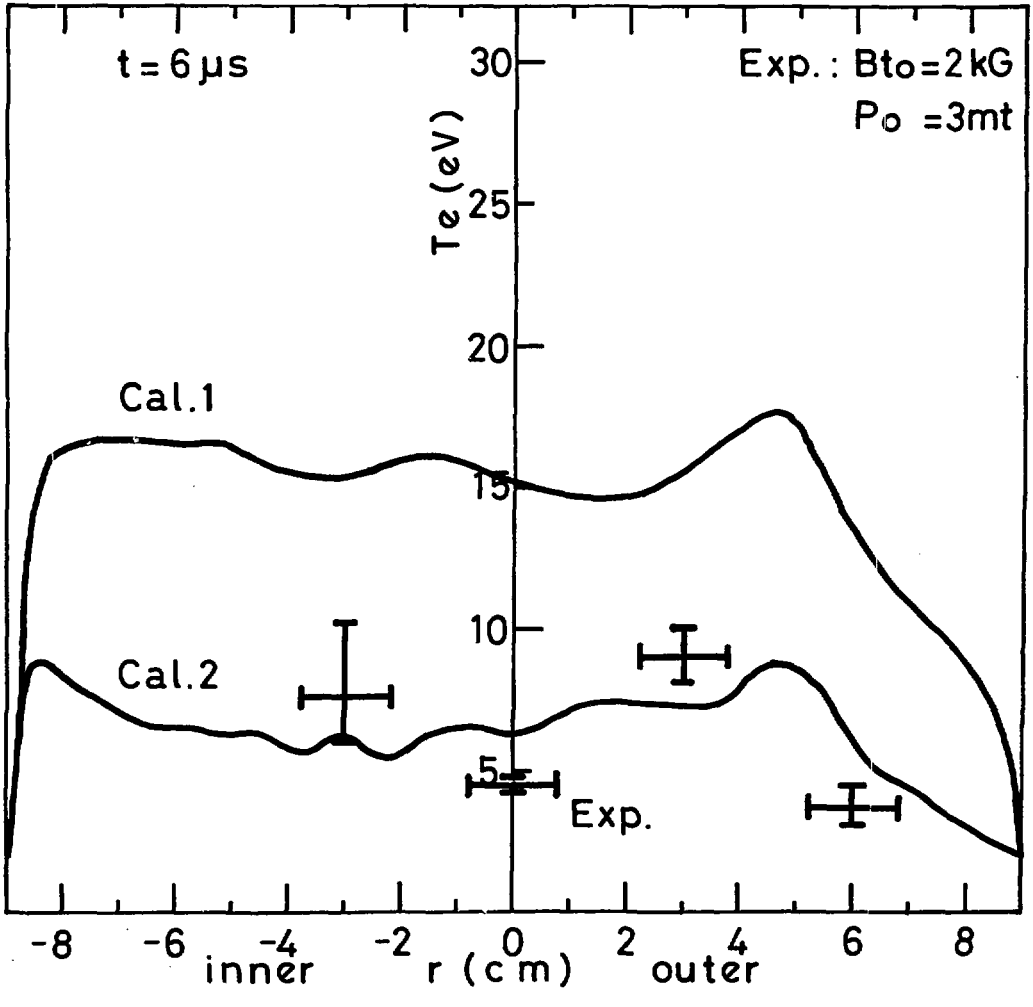
t = 6 μs
Exp. : Bto=2 kG
Po =3mt
Te (eV)
30
25
20
15
10
5
Cal.1
Cal.2
Exp.
-8
-6
-4
-2
0
2
4
6
8
inner
r (cm)
outer

Fig. 5 (b)

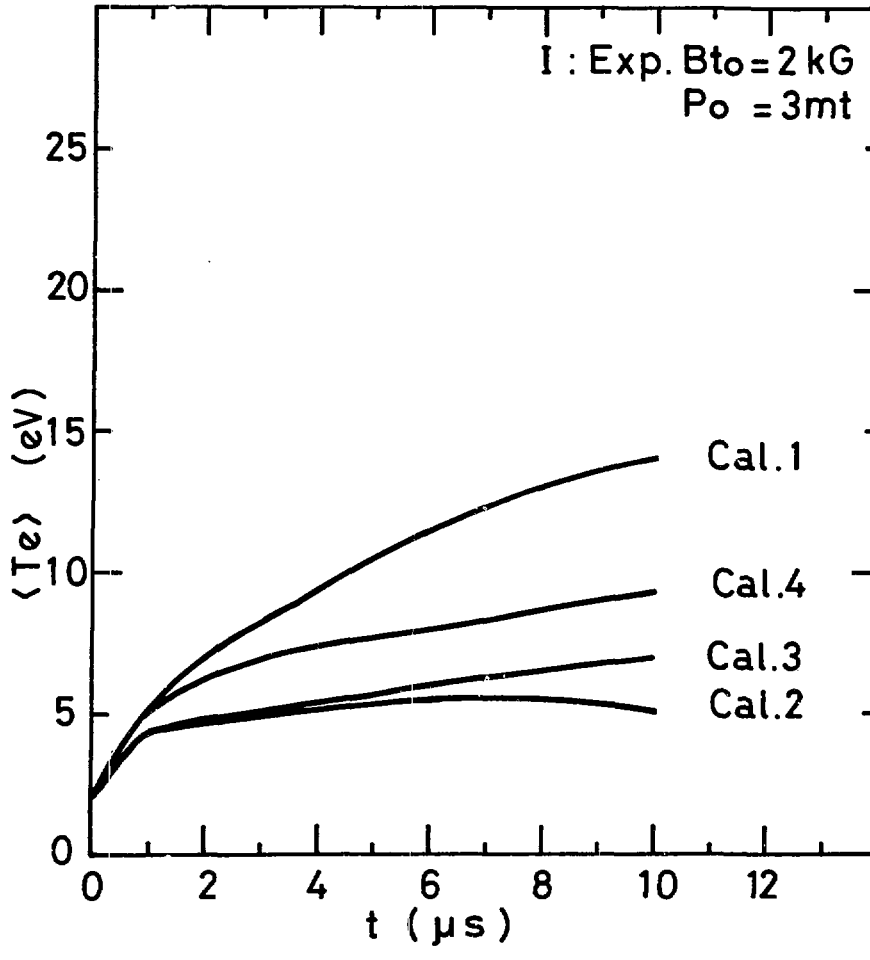
I : Exp. Bto = 2 kG
Po = 3mt
25
20
15
10
5
0
⟨Te⟩ (eV)
Cal.1
Cal.4
Cal.3
Cal.2
0
2
4
6
8
10
12
t (μs)

Fig. 6

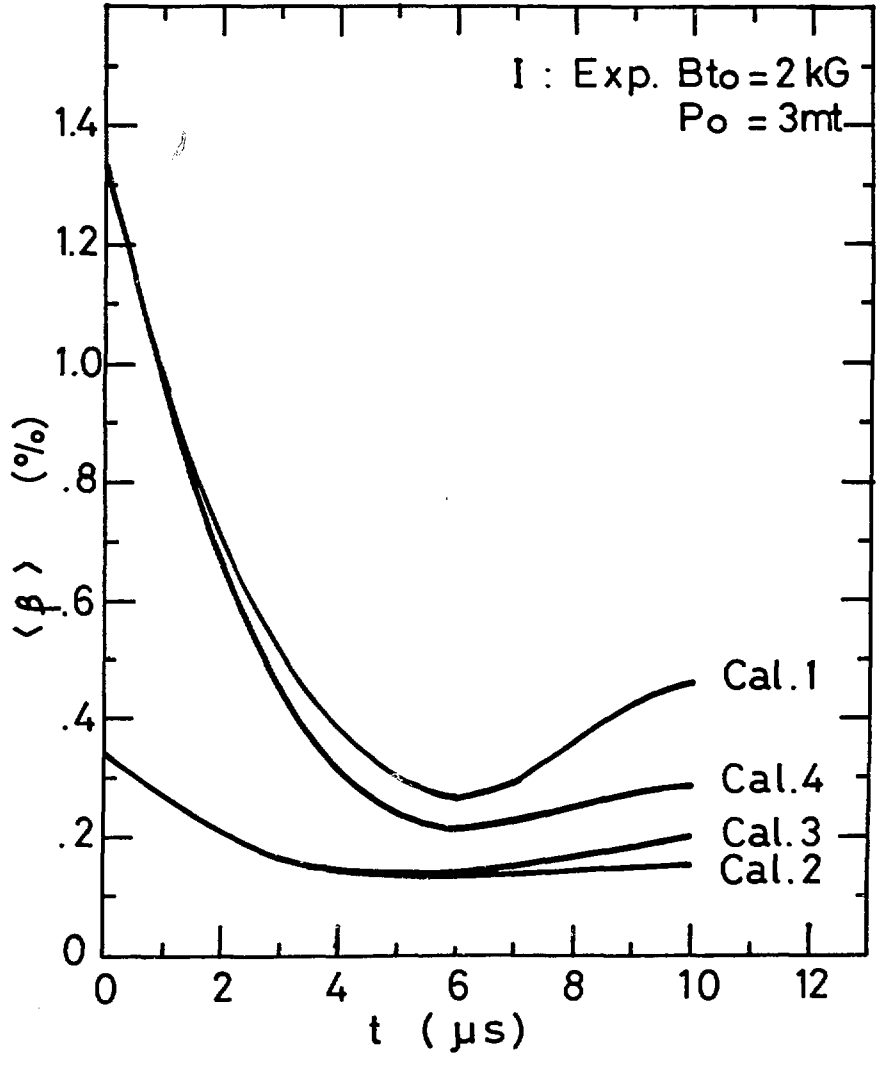
I : Exp. Bto = 2 kG
Po = 3mt
1.4
1.2
1.0
.8
.6
.4
.2
0
⟨β⟩ (%)
Cal.1
Cal.4
Cal.3
Cal.2
0
2
4
6
8
10
12
t (μs)

Fig. 7

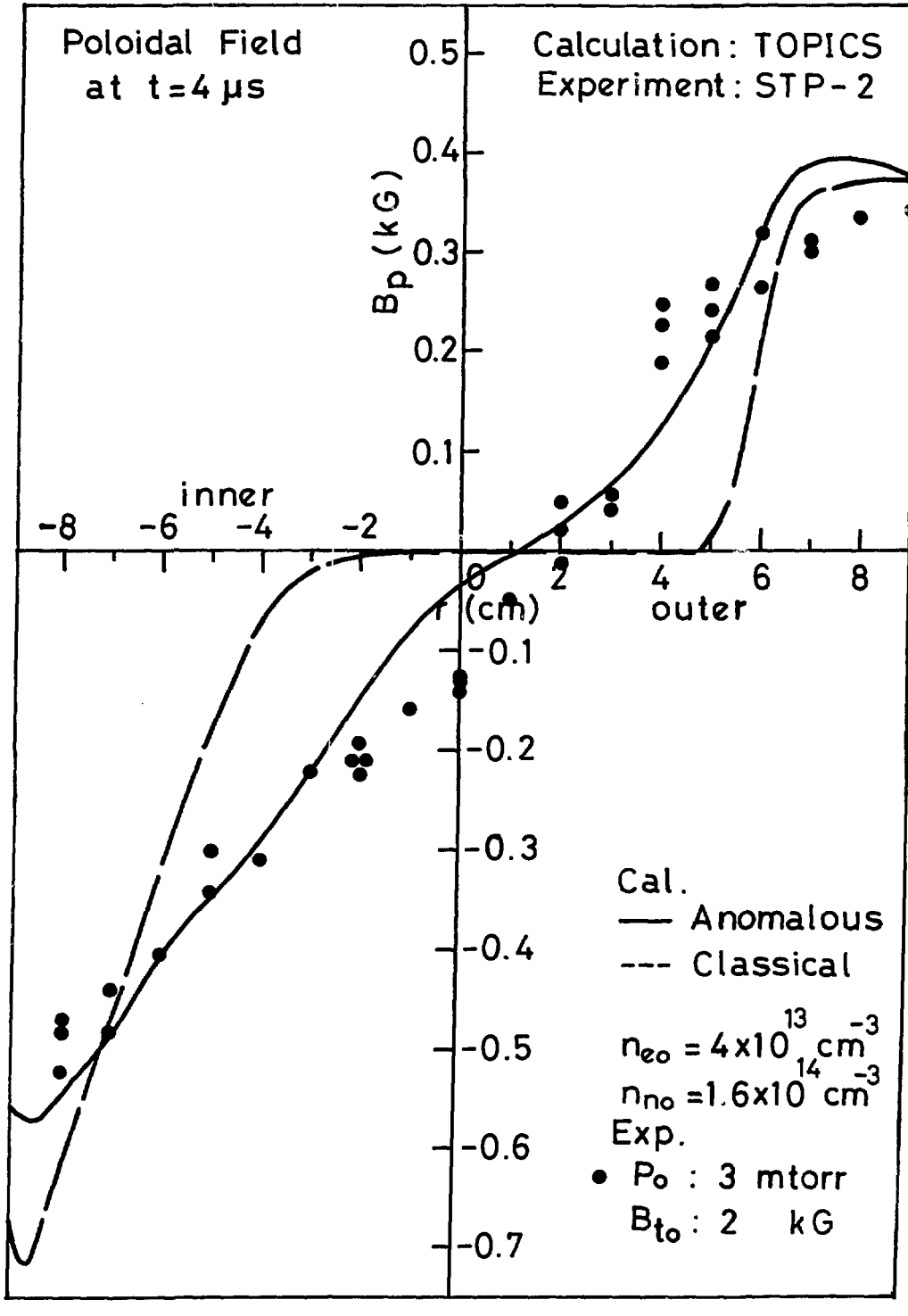
Poloidal Field
at t=4 μs
Calculation: TOPICS
Experiment: STP-2
B_p (kG)
0.5
0.4
0.3
0.2
0.1
inner
-8
-6
-4
-2
0
2
4
6
8
outer
r (cm)
-0.1
-0.2
-0.3
-0.4
-0.5
-0.6
-0.7
Cal.
Anomalous
Classical
$n_{eo} = 4 \times 10^{13}$ cm^{-3}
$n_{no} = 1.6 \times 10^{14}$ cm^{-3}
Exp.
P_o : 3 mtorr
B_{to} : 2 kG

Fig. 8 (a)

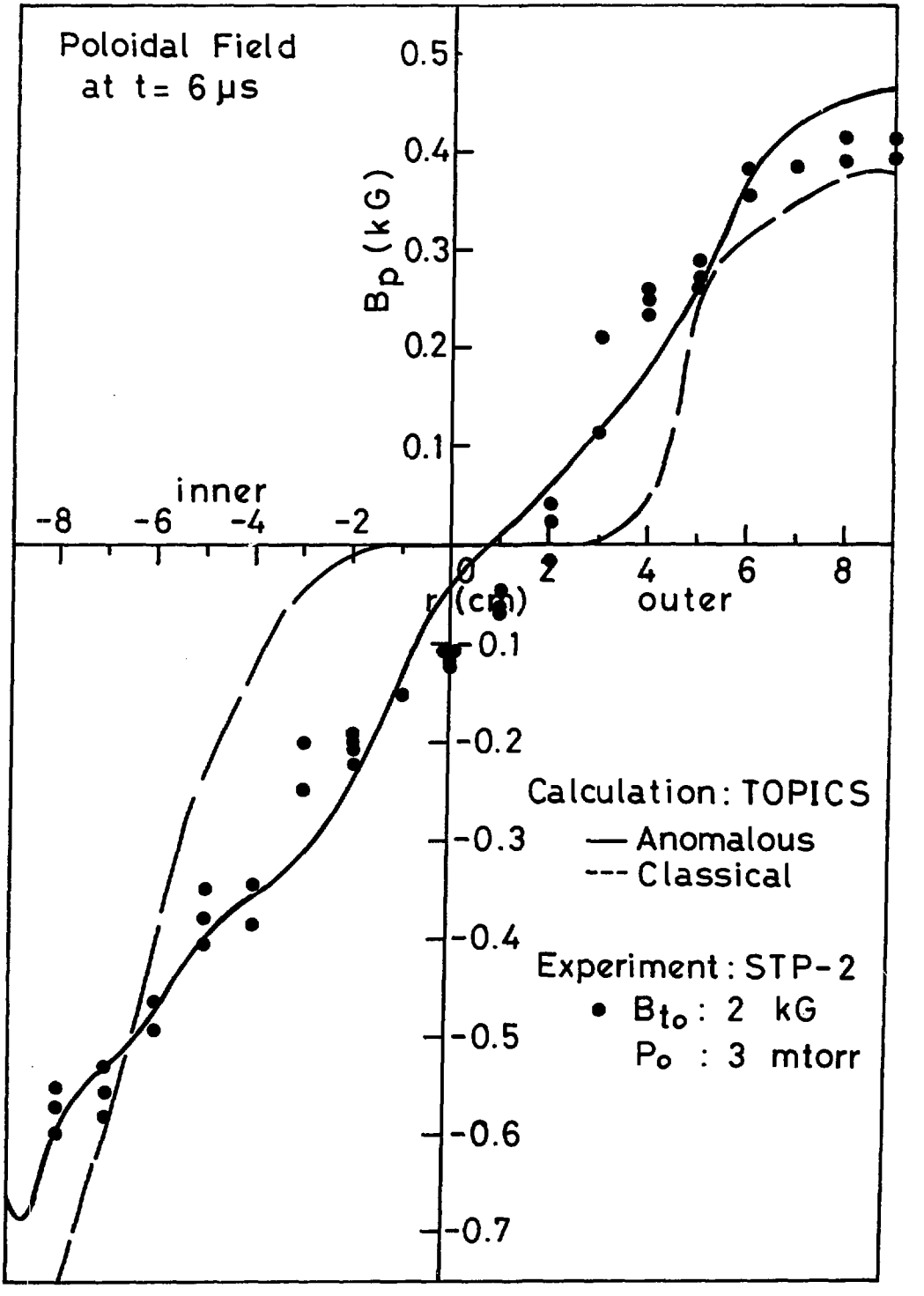
Poloidal Field
at t= 6 μs
B_p (kG)
0.5
0.4
0.3
0.2
0.1
inner
-8
-6
-4
-2
0
2
4
6
8
outer
r (cm)
-0.1
-0.2
-0.3
-0.4
-0.5
-0.6
-0.7
Calculation: TOPICS
— Anomalous
--- Classical
Experiment: STP-2
• B_{to} : 2 kG
P_o : 3 mtorr

Fig. 8 (b)

$\vec{V} : \vec{V}r + \vec{V}\theta$
(x 4 cm/μs)
at t = 4 μs
classical

Calculation: TOPICS
$n_{e0} = 0.4 \times 10^{14} cm^{-3}$
$n_{n0} = 1.6 \times 10^{14} cm^{-3}$
$B_{t0} = 2$ kG

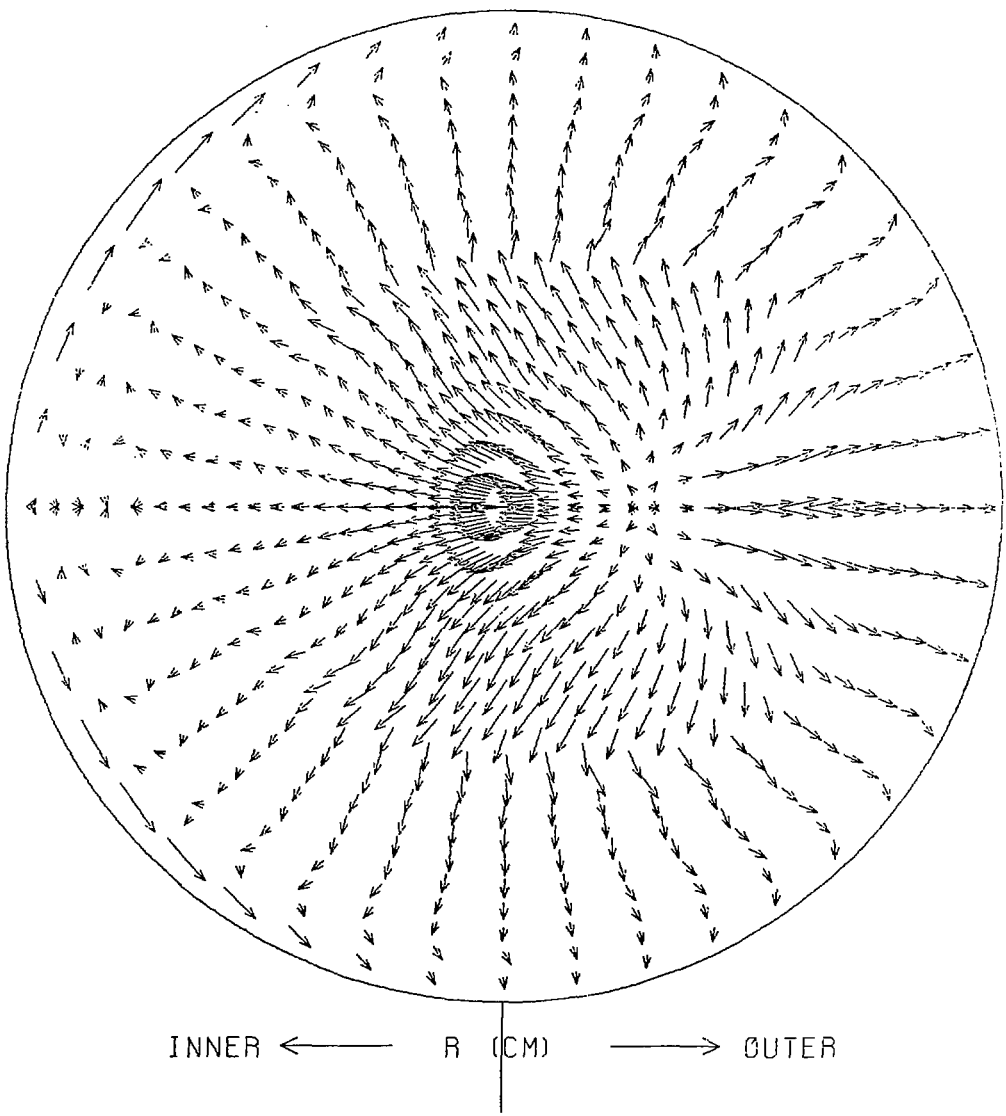

Fig. 9 (a)

$\vec{V} : \vec{V}r + \vec{V}\theta$
(x 4 cm/μs)
at t = 4 μs
anomalous

Calculation: TOPICS
$n_{e0} = 0.4 \times 10^{14} cm^{-3}$
$n_{n0} = 1.6 \times 10^{14} cm^{-3}$
$B_{t0} = 2$ kG

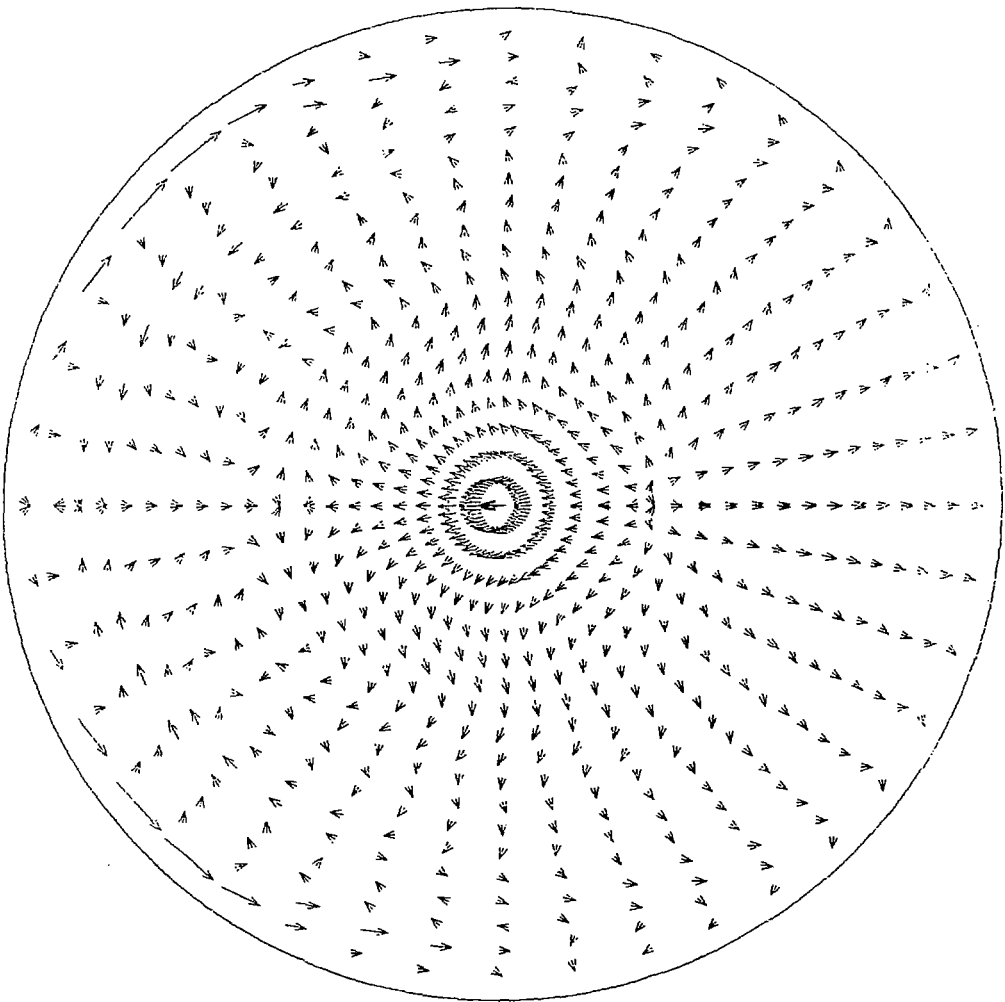

Fig. 9 (b)

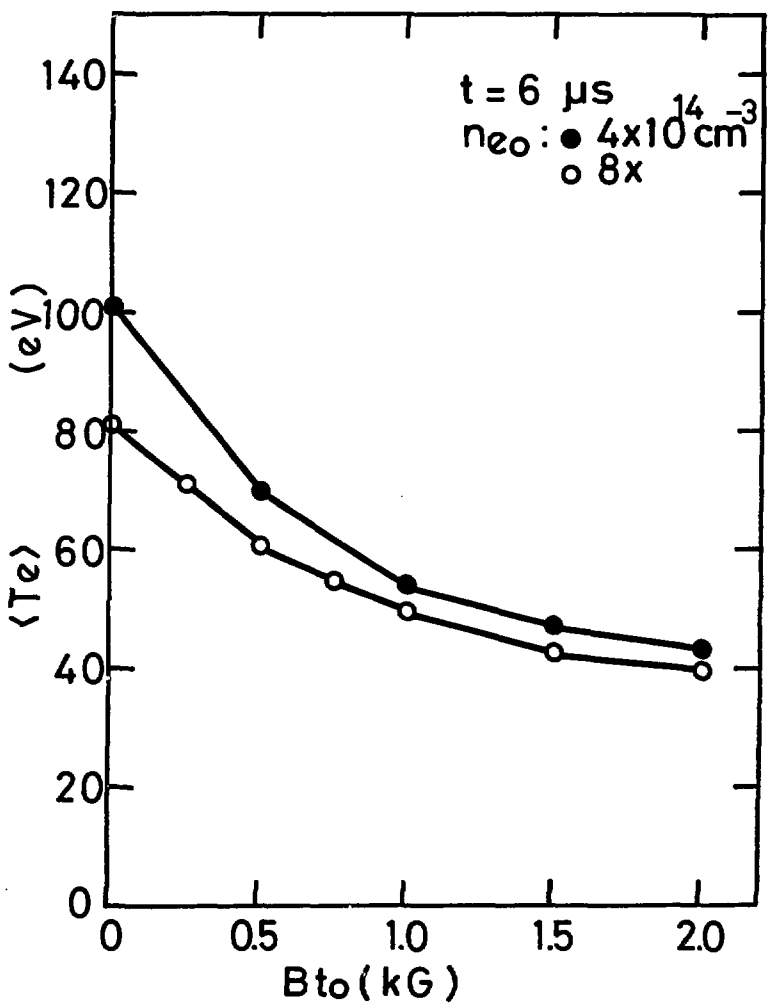
t = 6 μs
n_{eo} : ● 4x10^{14}cm^{-3}
o 8x
⟨Te⟩ (eV)
140
120
100
80
60
40
20
0
0
0.5
1.0
1.5
2.0
Bto (kG)

Fig . 10

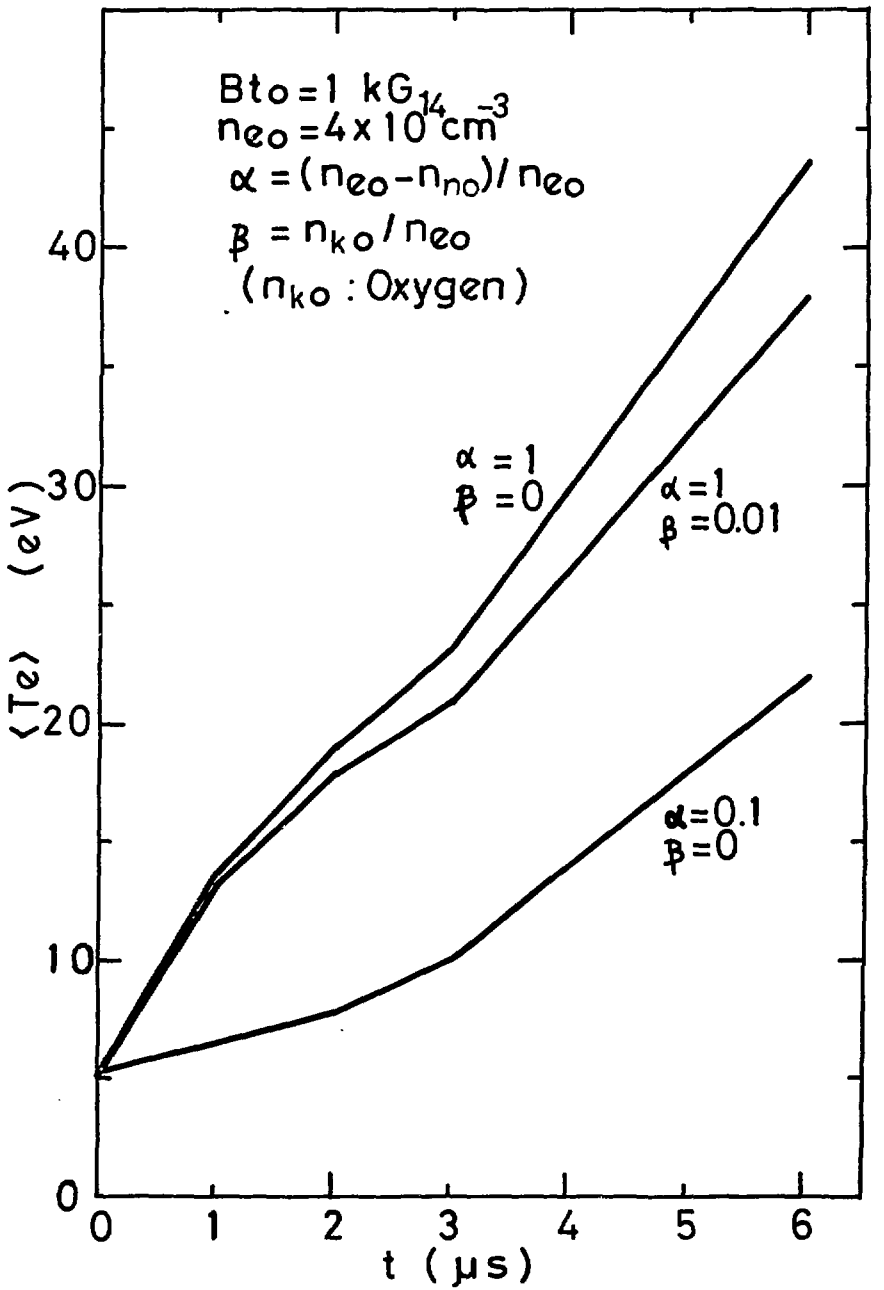
Bto=1 kG
neo=4x10^14 cm^-3
α=(neo-nno)/neo
β=nko/neo
(nko : Oxygen)
α=1
β=0
α=1
β=0.01
α=0.1
β=0
⟨Te⟩ (eV)
0
10
20
30
40
0
1
2
3
4
5
6
t (μs)

Fig. 11